J Solid State Electrochem (2008) 12:1301–1315
DOI 10.1007/s10008-008-0524-4

ORIGINAL PAPER

Efficient strategy for quality control of screen-printed carbon ink disposable sensor electrodes based on simultaneous evaluation of resistance, capacitance and Faradaic current by Fourier transform AC voltammetry

Alexander R. Harris · Jie Zhang · Anastassija Konash · Darrell Elton · Mark Hyland · Alan M. Bond

Received: 14 December 2007 / Revised: 29 January 2008 / Accepted: 30 January 2008 / Published online: 7 March 2008

Abstract Two types of mass-produced, screen-printed carbon ink-based macrodisc electrodes suitable for routine sensing applications have been fabricated. Microscopic examination of these carbon ink electrode surfaces reveals that their surfaces are both rough and highly heterogeneous, consisting of random arrays of carbon particles of different sizes, as well as binder. Consequently, they may suffer from a lack of reproducibility in their performance because of variable resistance, capacitance or electroactive area. Use of a Fourier transform AC voltammetric protocol involving application of periodic waveform obtained from summation of five sine waves of variable frequency enabled resistance and capacitance, as well as DC and AC Faradaic currents associated with the model processes FcMeOH $\rightleftarrows$ $FcMeOH^+ + e^-$ or $\left[Ru(NH_3)_6\right]^{3+} + e^- \rightleftarrows \left[Ru(NH_3)_6\right]^{2+}$ (where FcMeOH is ferrocene methanol) to be assessed from a single experiment. Such data, which may be obtained rapidly via this approach, are highly suitable for quality control assessment.

A. R. Harris · J. Zhang · A. Konash · A. M. Bond (✉)
School of Chemistry, ARC Center for Green Chemistry,
Monash University,
Clayton, Victoria 3800, Australia
e-mail: alan.bond@sci.monash.edu.au

D. Elton
Department of Electronic Engineering, Latrobe University,
Bundoora, Victoria 3086, Australia

A. R. Harris · M. Hyland
Oxford Biosensors Limited,
Oxford Industrial Park, Mead Road,
Yarnton, Oxfordshire OX5 1QU, UK

Keywords Thick-film carbon ink electrodes · Fourier transform AC voltammetry · Resistance · Capacitance · Quality control of electrode fabrication

Introduction

Electrochemical sensing of glucose and other biologically important molecules now represents a widely used form of routine analysis. The simplicity, sensitivity and selectivity of this method [1, 2], combined with the ability to use battery-operated instrumentation, has enabled this form of electroanalysis to be taken outside the conventional laboratory and into less traditional situations such as doctors' surgeries, homes and remote locations. Matrices that now can be examined with this technology by non-electrochemical experts include blood, urine, industrial waste, environmental samples and food products [3, 4]. In the case of low-cost, mass-produced voltammetric or amperometric sensors developed for measurement of blood analytes, the cell design and instrumentation must be simple and the electrodes should be inexpensive, robust and disposable, require little to no preparation and only need the use of small sample volumes. The traditional use of 10 mL or even greater solution volumes in cell configurations containing macrodisc glassy carbon (GC) or other forms of working electrode, large surface area platinum mesh counter electrodes and conventional Ag/AgCl reference electrodes is therefore not feasible.

Screen-printing is used to fabricate electronic devices such as displays, printed circuit boards and semiconductor devices, and also nowadays forms the basis of fabrication of most commercially available electrodes used for electro-

chemical biosensing [3–5]. The key issues in screen-printing of electrodes include ink conductivity, surface topography and functionality, registration (alignment of sequential printed layers) and print quality. Not surprisingly, much recent research activity in the electrochemical biosensing area is aimed at optimisation of manufacturing procedures inherently necessary to achieve low-cost, small-volume, highly reproducible and reliable mass-produced devices.

In this paper, we describe the characterisation of mass-produced, screen-printed macrodisc electrodes by optical microscopy, scanning electron microscopy (SEM), energy-dispersive X-ray analysis (EDX) and secondary-ion mass spectrometry (SIMS). Given the need to generate these electrodes on a large scale, simple strategies for quality control are also introduced based on simultaneously measured Faradaic current, resistance and capacitance by Fourier transform (FT) AC voltammetry. All these characterisation and quality control approaches are general and, hence, should also be applicable to all electrode geometries generated by screen-printing technology.

Materials and methods

Electrode fabrication

Two distinctly different design types of screen-printed electrodes (SPE) were produced. In type 1, the electrode fabrication procedure (Fig. 1) was as follows: a plastic substrate was used to provide the platform, onto which the various inks (supplied by Ercon, DuPont or Coates) were printed. In step 1, lines of silver ink (Coates 26–8204) were printed (Fig. 1ai). In step 2, carbon ink (DuPont E104195–80A) was printed over the top of the silver lines with round pads produced at the end to form the working electrode surface (Fig. 1aii). The underlying silver ink is used to reduce the resistance of the working electrode, but it must be completely covered by the carbon ink. In step 3, an insulating layer (dielectric ink Ercon E6165–116) is printed over the 'legs' of the electrodes so that only the pads and a length of the legs for connection to the instrumentation remain exposed (Fig. 1aiii). In step 4, to create a reference electrode, a silver chloride layer (Ercon E0430–128) is screen-printed onto the central of the five carbon pads. After this procedure, the strip has four macrodisc electrodes and a central Ag/AgCl reference electrode (Fig. 1b). Each of the steps 1 to 3 was followed by 1 h curing in the oven at 100 °C. As can be seen from Fig. 1b, in step 3 (Fig. 1aiii) of type 1 electrodes, the dielectric does not perfectly match with printed carbon discs covering parts of the round pads and leaving some of the legs and supporting plastic substrate (crescent-like white parts around carbon pads) exposed.

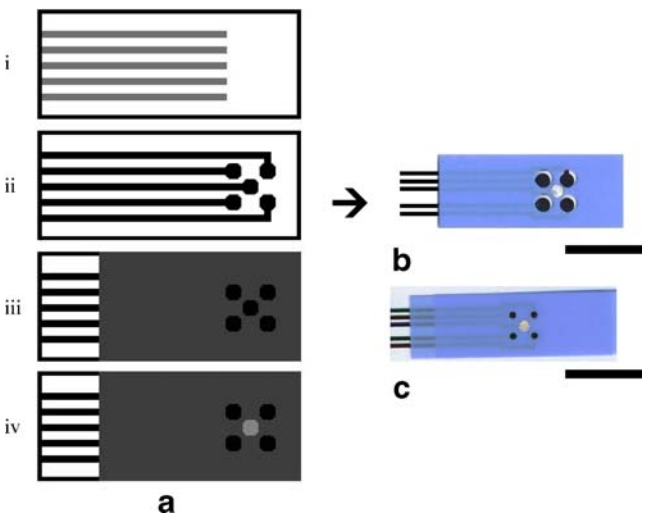

Fig. 1 **a** Top view illustrating the method for manufacturing screen-printed disc electrodes, from top to bottom, *i* silver tracks printed onto a plastic substrate, *ii* carbon tracks and pads added, *iii* a dielectric film masking the electrode legs, *iv* a silver/silver chloride reference is printed; **b**, **c** images of SPE 1 and 2, respectively (*scale bar* is 1 cm)

Type 2 SPEs were manufactured by omitting step 1 (Fig. 1ai) but following step 2 up to step 4 of the above procedure. However, the screen used to print the dielectric layer in step 3 had smaller through-holes, which meant that dielectric inks covered the carbon pads, which resulted in a significantly smaller and visually more reproducible electrode area (Fig. 1c). This type of electrode was therefore expected to exhibit a more reproducible electroactive area, but the absence of the silver ink was expected to result in a higher electrode resistance. Type 1 SPEs were printed using DuPont E104145–80A carbon ink, while DuPont BQ242 ink was used for type 2 SPEs. An average geometrical area of eight carbon pad electrodes from both designs (assumed to be planar) was determined by analysis of images captured by optical microscopy. The images were printed out and divided into squares, which were then counted. The dimensions of the images were calibrated against those from atomic force microscope tips of known dimensions captured at the same time. Type 1 SPEs had an average geometrical area of 3.16 ± 0.10 mm^2, while that for type 2 SPEs was 0.433 ± 0.02 mm^2.

Large numbers of electrode arrangements were produced simultaneously on the plastic substrate in each screen-printing run. Individual strips (Fig. 1b and c) were cut out from the backing sheet and inserted into a standard electrical connector via the electrode legs to give a configuration in which each of the four carbon pads and the Ag/AgCl reference electrode could be controlled

electrochemically. The SPE arrays were dipped directly into the test solution. In the case of a 3-electrode potentiostated experiment, one of the carbon pad electrodes was used as the working electrode, the Ag/AgCl layer was the reference electrode and platinum gauze was placed in solution to become the auxiliary electrode. In two-electrode experiments, one carbon pad was used as the working electrode and the counter and reference electrode inputs of the potentiostat were connected to the Ag/AgCl reference electrode.

Chemicals

Potassium chloride (BDH), ferrocenemethanol (FcMeOH, Aldrich) and hexaminеruthenium(III) chloride ($[Ru(NH_3)_6]Cl_3$, Strem) were used as received from the manufacturer. Doubly distilled water was used for the preparation of electrolyte solutions.

Instrumentation and procedures

SIMS experiments were undertaken with a MiniSIMS (Millbrook Instruments) instrument. SEM images were obtained with a JEOL 840A system containing an Oxford Link EDX system for elemental analysis. The DC cyclic voltammetric experiments were performed with an Autolab PGSTAT100 (ECO-Chemie) electrochemical workstation.

SPEs were manufactured as detailed above. Reference data were obtained with 3-mm-diameter GC working electrodes (IJ Cambria, BAS), polished with 0.3 μm alumina slurry on a polishing cloth (Microcloth), dried with tissue paper (Kimwipe) and rinsed with acetone, in combination with a Ag/AgCl (aqueous 3 M NaCl) reference electrode and a platinum mesh auxiliary electrode. In initial experiments, a new GC electrode (GC A) was used that was flat and planar. In a second set of experiments, the GC electrode used (GC B) was one that was extensively employed in this laboratory for more than 3 years. In this case, the Teflon holder has been polished to a level where the GC disc was raised above the holder and was neither flat nor planar. The quality control procedure developed in this work should be able to distinguish differences in performance between these two types of GC electrode.

All voltammetric experiments were performed at 20± 2 °C without removal of oxygen from the solution. Simulations of DC cyclic voltammetry at GC and SPE electrodes were undertaken with DigiSim software (Bioanalytical Systems). In some experiments, 510 and 1,000 Ω resistors were connected in series to the working electrode placed in 0.2 M KCl solution. In all experiments performed, a high concentration of supporting electrolyte 0.2 M KCl was used to minimise solution resistance, so that the resistance values strongly reflect the resistance of the screen-printed carbon electrodes and contact resistance, which are the important terms in quality control of SPEs.

FT AC voltammetric measurements used to characterise the voltammetric performance and determining the resistance and capacitance (C) of the electrochemical cell configurations was undertaken with custom-built instrumentation [6]. In the configuration used in this study, a digital processing system based on an 18-bit stereo digital–analog converter generates a potential waveform that consists of the summation of a highly linear DC ramp (E_{dc}) and five sine waves (E_{ac}) of known frequency (ω), amplitude (ΔE) and phase (Fig. 2a), which is applied to a conventional op-amp-based potentiostat.

The FT AC experiment was arranged so that exactly 2^N pairs (convenient for FT processing) of I–E data points were collected at a constant sampling rate (25.6 μs), digitally corrected for instrumental offset and phase shift and then stored as a raw data file. The 'exactly 2^N pairs of I–E data points' condition in any given potential window was satisfied by adjustment of the scan rate of the applied potential waveform. This outcome was accomplished via an 18-bit stereo analog–digital converter preceded by a software-adjustable current amplifier (five decade ranges covering 3 mA down to 30 nA full-scale). After collection of the total (DC and AC) current as a function of time (Fig. 2b), an FT algorithm was used to convert the time domain data into a power spectrum (frequency domain) (Fig. 2c and d). Separation of fundamental harmonics of each of the five applied AC frequency components and the DC component, if required, is achieved by selecting a frequency band that retains most of the energy (~5 and 18 Hz, respectively), and zeroing the remaining portion before applying an inverse FT to give data of the kind in Fig. 2e (DC component) and f (one of the base AC components). Many other higher harmonics and frequency sum and difference are generated, as noted from inspection of the power spectrum (Fig. 2c). Furthermore, mains frequency (50 Hz) is introduced into the system from various electrical sources. These terms prevent the use of many frequencies when attempting to obtain five fully resolved AC fundamental components with their required bandwidth. The use of small amplitude (~5 mV) AC signals reduces the power of the higher harmonic and frequency sum and difference contributions (Fig. 2d). A Matlab routine was used to generate the five frequencies selected as being suitable for quality control purposes and can generate their fundamental harmonics without a significant contribution from other fundamental, second harmonic or other frequency sum and difference terms.

The FT AC experiment was simulated using a previously published procedure [7]. The applied potential [$E(t)$, t is

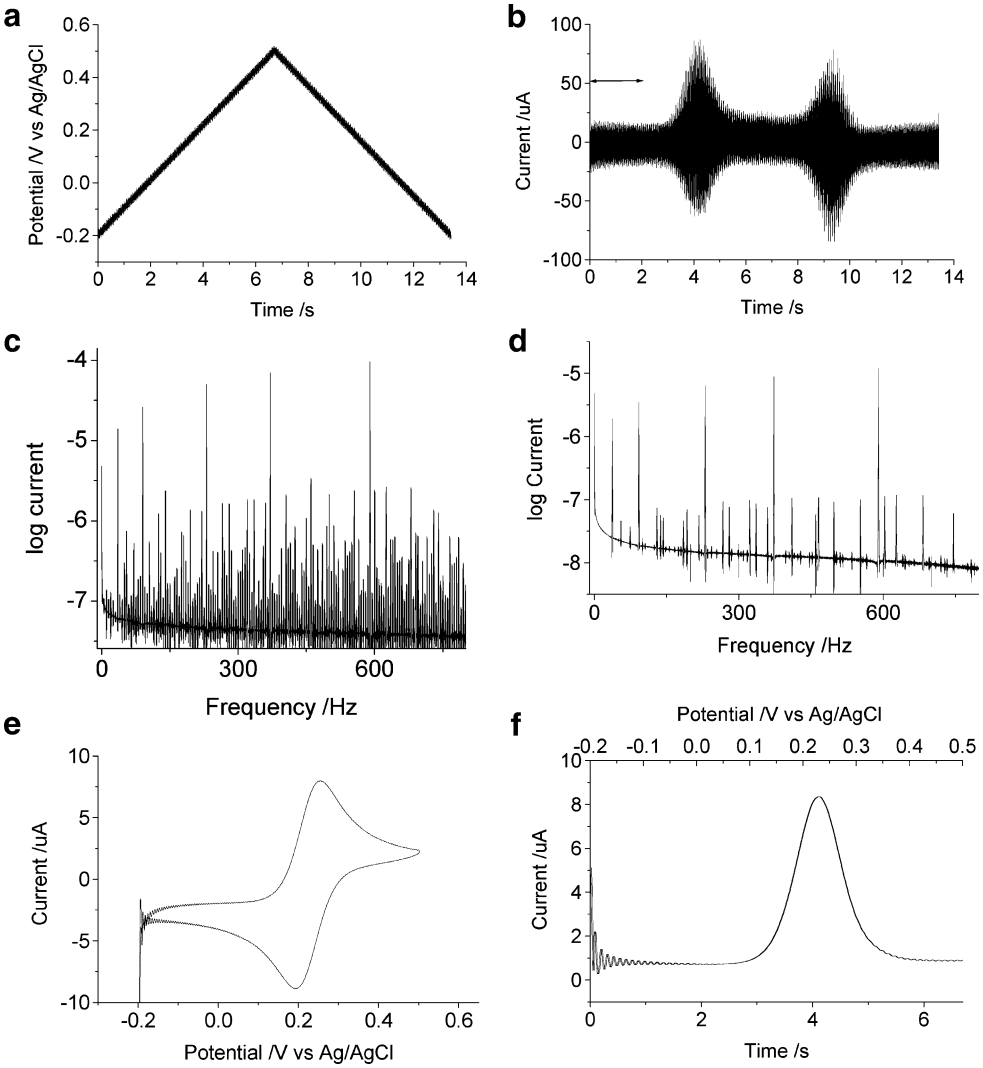

Fig. 2 Typical FT AC voltammetric data obtained for oxidation of 0.5 mM FcMeOH in 0.2 M KCl at a GC A electrode with a scan rate of 104.31 mV s^{-1} **a** applied waveform consisting of a DC ramp over which is superimposed five sine waves, **b** measured current–time response, **c** and **d** power spectrums obtained after Fourier transformation of large and small amplitude AC voltammetry, **e** DC component after inverse Fourier transformation and **f** one AC component after inverse Fourier transformation. *Arrow* in **b** represents the time region used for background fitting and calculation of R_s and C

time] in the present case is a combination of a ramped DC waveform [$E_{dc}(t)$, scan rate v] and five sine waves of frequencies ($\omega_1,\omega_2,\ldots,\omega_5$) [$E_{ac}(t)$] to give:

$$E(t) = E_{dc}(t) + E_{ac}(t) \tag{1}$$

Where

$$E_{ac}(t) = \Delta E\sin(\omega t_1) + \Delta E\sin(\omega t_2) + \Delta E\sin(\omega t_3) + \Delta E\sin(\omega t_4) + \Delta E\sin(\omega t_5) \tag{2}$$

$$E_{dc}(t) = E_1 \pm vt \tag{3}$$

Calculation of uncompensated resistance and capacitance

Traditionally, to measure the resistance (R) and capacitance (C), the method of impedance spectroscopy is employed using a multifrequency waveform under conditions of constant DC potential [8]. In contrast, in FT AC voltammetry, the DC potential is scanned rapidly. For the purpose of quality control assessment of screen-printed carbon ink electrodes, the ability to use a rapid scanning method that also readily gives DC and AC Faradaic current (electroactive electrode area) and R and C values at all potentials of interest from a single experiment is an attractive approach.

To use the FT AC voltammetric approach for quality control purposes, it was assumed that R and C values of SPEs could be derived from the data obtained in a potential region where there is no Faradaic current and use of the simplest possible equivalent circuit available (Fig. 3), in which a resistor (R_s) and capacitor (C) are connected in series. It is noteworthy that R_s is not necessarily equal to the true value of the uncompensated resistance (R_u) but can be used as an approximation of R_u. Nevertheless, this approximation is adequate for quality control purposes

where the ability to detect differences in the resistance rather than absolute values is more important. Under these assumptions, and using an algorithm presented in the Appendix, one can obtain R_s and C values from Eqs. 4 and 5:

$$R_s = \frac{1}{\omega C \tan(\phi)} = \frac{1}{|Y|\sqrt{\tan^2(\phi)+1}} \quad (4)$$

$$C = \frac{1}{\omega}|Y|\sqrt{1+\frac{1}{\tan^2(\phi)}} \quad (5)$$

Where ω is a given angular perturbation frequency, ϕ is the phase angle of admittance (Y) and $|Y|$ is a magnitude of admittance (Y). Equations 4 and 5 were derived from analysis of the impedance (Z) of the equivalent circuit shown in Fig. 3 (refer to Appendix for more details). Equations 4 and 5 are equivalent to the ones available in standard textbooks on electrochemistry [9–11], where limiting conditions and approximations involved are described in detail. It is of course recognised that carbon electrodes are actually complex chemically modified electrodes (see later) and that the simple RC network used for the equivalent circuit analysis represents only a modest approximation of the actual situation. A theoretical description of more complex equivalent circuits and approximations introduced by using these equations under finite scan rate conditions is available [12]. However, because it is the reproducibility of the data rather than absolute values of resistance and capacitance that is critical in quality control, the simple RC approach was adopted.

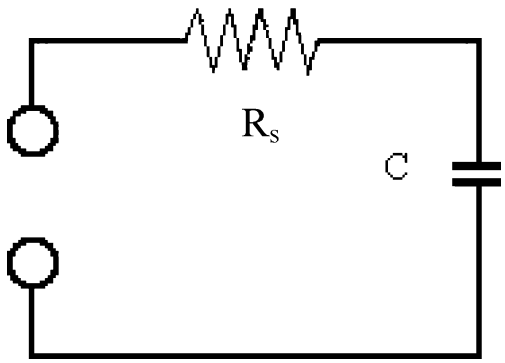

Fig. 3 Equivalent circuit representation of the two-parameter RC model employed to fit the background current obtained under conditions of FT AC voltammetry

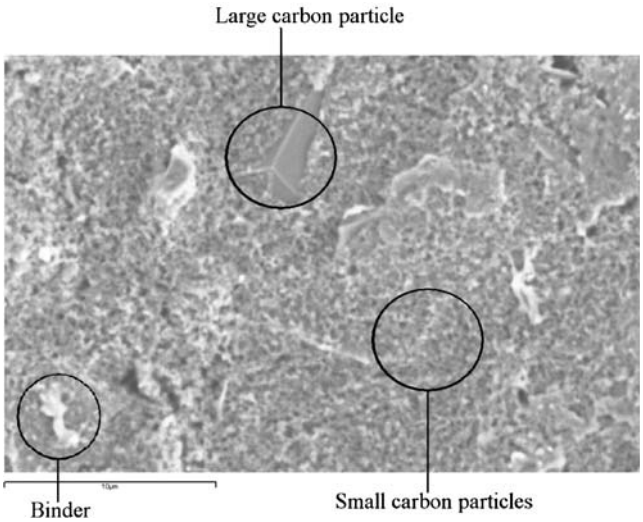

Fig. 4 SEM image obtained for SPE 1. Scale bar is 10 μm

Results and discussion

Microscopy and SIMS of SPEs

SEM images of the surface of SPE used in design 1 fabricated for the present studies (Fig. 1b) indicated the expected heterogeneity in their surface structure (Fig. 4). These images revealed that the carbon inks from which they were prepared contained two sizes of carbon particles (large ~5 μm and small <1 μm diameters) incorporated into a binder matrix. These characteristics are generally consistent with those reported for other SPEs [13–16], but they do vary significantly with the source of the ink. As the binder is insulating, the observed surface material distribution results in an array of micro-electrodes (carbon particles) separated by non-conductive regions (binder) [15]. The surface roughness and heterogeneous nature of the electrode surface is expected to affect the electroactive electrode area and the nature of the voltammetry [16]. Consequently, voltammograms could be significantly different from those predicted for model systems based on an ideal planar macrodisc electrode.

The SIMS technique has a sampling depth of 1–5 nm. Analysis of specific m/z values detected by scanning over the region of the four carbon ink macrodisc and Ag/AgCl electrodes area in design 1 (Fig. 1b) is presented in a form that gives a light colour for a large m/z count at each location (Fig. 5). The dielectric layer is high in $C_3H_5^+$ (as an indicator of aliphatic carbon), as expected Ag^+ and Cl^- are present at high levels on the Ag/AgCl reference electrode region, and O^-, C_4^- (an indicator of graphitic carbon) and CN^- are present on the carbon ink electrode surfaces but little Cl^- [as an indicator of a chlorinated binder such as poly(vinyl chloride)]. However, EDX

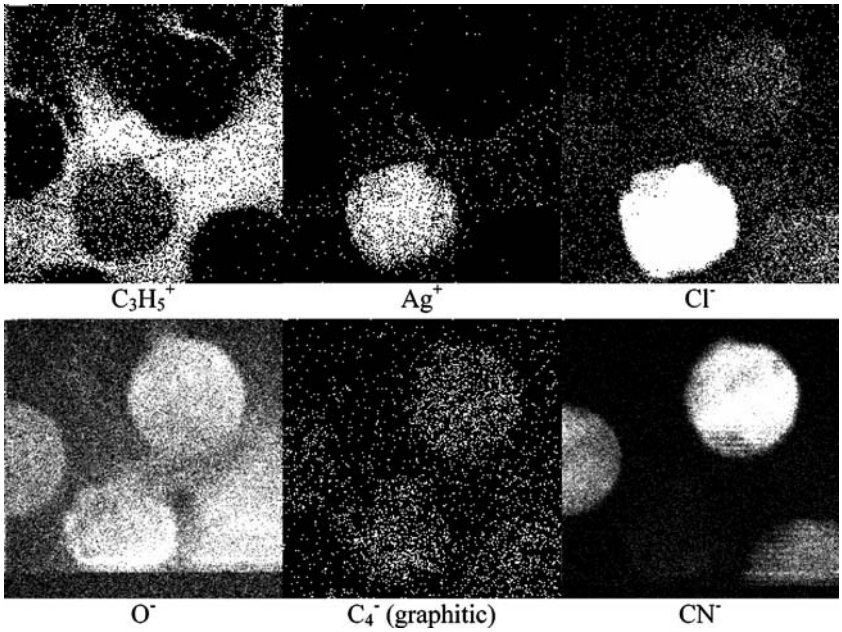

Fig. 5 SIMS images of SPE 1 with the four carbon electrodes around the Ag/AgCl reference electrode. A high m/z count appears white

analysis, which has a much larger sampling depth of over 1 μm, indicates the presence of only carbon, oxygen and low levels of sulphur. Thus, CN^- detection, because it is confined to the surface, possibly is a result of chemical reaction between carbon and airborne agents, residual solvent present in the ink or a contaminant. Comparison of SEM images and EDX analysis from two different plastic substrates used as the electrode assembly platform (one being white due to the presence of barium sulphate as a whitening agent and the other clear) indicated that the ink surface on the white substrate was less uniform and contained $BaSO_4$. Consequently, only the clear backing sheet was used for preparation of electrodes evaluated in this study.

Analysis of electrode surfaces printed using inks obtained from a range of suppliers revealed significant differences in carbon particle size, distribution and binder. Clearly, electrode performance is expected to depend on the source of ink and binder, as well as design. However, ultimately, it is the reproducibility of the electrode performance that matters in sensing applications and resistance, capacitance and Faradaic current details are the key indicators that may be used to establish the reproducibility of electrode manufacture.

DC cyclic voltammetry

Initially, DC cyclic voltammetric studies, using a new GC A electrode, and reduction of a 5-mM solution of $[Ru(NH_3)_6]Cl_3$ in 0.2 M KCl were undertaken (Fig. 6a) to provide a basis for comparison with the carbon ink screen-printed disc electrodes. A mid-point potential (E_{mid}) of −167 mV vs Ag/AgCl (3 M NaCl) was obtained, as calculated from the average of the reduction (E_p^{red}) and oxidation (E_p^{ox}) peak potentials as follows: $E_{mid} = \left(E_p^{red} + E_p^{ox}\right)/2$. As well as exhibiting the reversible [Ru

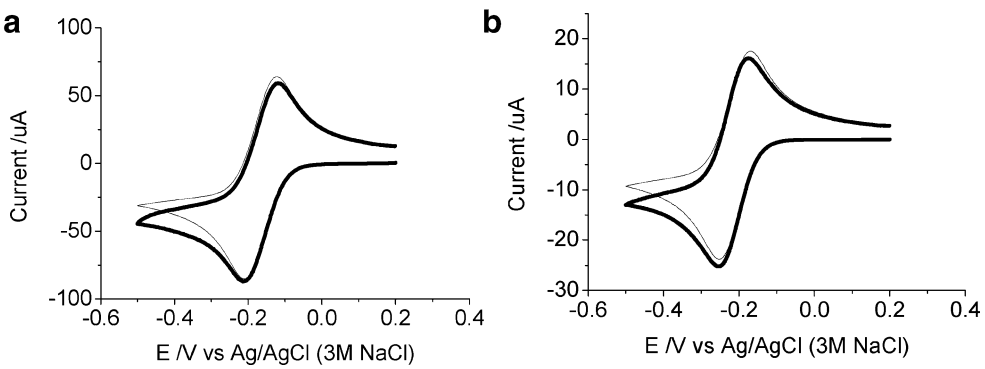

Fig. 6 Simulated and experimental cyclic voltammograms obtained for reduction of 5 mM $[Ru(NH_3)_6]Cl_3$ in 0.2 M KCl in a three-electrode configuration at a scan rate of 100 mV s^{-1} **a** using a GC A working electrode and **b** SPE 1. *Thick line*, experimental data; *thin line*, simulation. See text for details

$(NH_3)_6]^{3+/2+}$ process, the voltammetry also includes the onset of the irreversible oxygen reduction process in the negative potential region [13, 16]. The high concentration of $[Ru(NH_3)_6]Cl_3$ used in these experiments meant that the Faradaic current is large and dominates over the background current. These conditions enabled both the Faradaic current and uncompensated resistance (R_u) contributions as well as the electrode area to be ascertained by comparison to DC cyclic voltammograms simulated assuming a reversible charge transfer process, a diffusion coefficient of 6.7×10^{-6} cm^2 s^{-1} [11] and other known parameters. Simulated voltammograms using a R_u value of 100 Ω and electrode area of 7.2 mm^2 (close to the geometric area of 7.065 mm^2) were in satisfactory agreement with experimental voltammograms (Fig. 6a) (background current from onset of oxygen reduction introduced uncertainties at negative potentials [13, 16]). Peak-to-peak separation (ΔE_p) of the reduction and oxidation peak potentials, particularly when the concentration of $[Ru(NH_3)_6]Cl_3$ is lowered to 0.5 mM (Table 1), are close to the value of 56 mV expected for a reversible process at 20 °C, implying that IR_u problems are minimal when using the 3-electrode planar macrodisc GC electrode configuration.

Cyclic voltammetry (Fig. 6b and Table 1) derived from screen-printed carbon ink electrode 1 using a 5- or 0.5-mM solution of $[Ru(NH_3)_6]Cl_3$ in 0.2 M KCl was also undertaken. However, on this occasion, both two- and three-electrode configurations were employed because use of a two-electrode, non-potentiostatic device is attractive for low-cost sensor applications. In this case, the potential of the Ag/AgCl reference electrode is determined by the chloride activity provided by 0.2 M KCl electrolyte rather than by the 3 M NaCl present in the conventional reference electrode, resulting in the shift in the mid-point potential. In addition, in some instances, deposition and stripping peak from contaminant Ag/AgCl on carbon pads was observed. As expected, R_u and, hence, IR_u are significantly larger in the two-electrode configuration than in the three-electrode configuration, as evidenced by larger ΔE_p values obtained in the two-electrode mode for reduction of 5 mM $[Ru(NH_3)_6]$ (Table 1). R_u in the three-electrode mode is basically derived from the resistance of the carbon ink electrode, contact resistance and solution resistance between the working and reference electrodes, whilst additional resistance terms from the Ag/AgCl reference electrode, contact resistance and solution are present when a two-electrode configuration is employed. Decreasing the $[Ru(NH_3)_6]^{3+}$ concentration to 0.5 mM decreases the magnitude of the Faradaic current and, hence, the effect of IR_u and leads to almost ideal reversible behaviour [ΔE_p=65–70 mV (Table 1)] at both GC and SPEs when used in three-electrode mode.

The smaller electrode area of SPE 2 compared to SPE 1 decreases the current magnitude. However, design 2 gives rise to much larger ΔE_p values (Table 1), so the IR_u drop effect is larger. This is attributed to the absence of the silver layer and, hence, higher leg resistance, which is not removed by use of a three-electrode configuration. Simulated cyclic voltammograms (see Fig. 6b with an electroactive electrode area of 2.2 mm^2) with an uncompensated resistance of 300 Ω matched closely with experimental data obtained for SPE 1 in the three-electrode configuration using $[Ru(NH_3)_6]^{3+}$ concentration of 5 mM and the scan rate of 100 mV s^{-1}. Noteworthy is the observation that a much higher resistance (R_u=3,200 Ω) was required to simulate cyclic voltammograms obtained with the same concentration and scan rate conditions at SPE 2, again consistent with the high resistance of the carbon ink legs [17], which highlights the value of the underlying silver ink layer in design 1. Interestingly, the above simulations of SPEs were made with a theoretical model assuming linear diffusion and a planar electrode. In practice, the SPEs are highly heterogeneous and the surface is rough, so the overlap of the diffusion layers must be extreme.

Use of the FT method and simultaneous evaluation of R_s, C and DC and AC Faradaic current requires use of data over a wide potential range. However, it is recommended that R_s and C should be determined from the data where no Faradaic current is present. As can be seen in Fig. 6a and b, the onset of the irreversible oxygen reduction process is evident at more negative potentials in addition to the $[Ru(NH_3)_6]Cl_3$ redox process [13, 16], which can cause uncertainties in data analysis. For quality control purposes, routine removal of oxygen by degassing the solution with nitrogen was not considered appropriate. Thus, FcMeOH, which has an E_{mid} value of 225±5 mV vs Ag/AgCl (3 M NaCl) and is well removed from the oxygen region, was also considered for use as an

Table 1 Cyclic voltammetric characterisation of GC and screen printed disc electrodes in 0.2 M KCl solution with scan rate of 100 mV/s

$[Ru(NH_3)_6]Cl_3$/mM	Electrode and configuration	ΔE_p/mV
5	GC A—3-electrode mode	70
0.5	GC A—3-electrode mode	60
5	SPE 1—2-electrode mode	150
5	SPE 1—3-electrode mode	75
0.5	SPE 1—2-electrode mode	100
0.5	SPE 1—3-electrode mode	70
5	SPE 2—2-electrode mode	160
5	SPE 2—3-electrode mode	100
0.5	SPE 2—2-electrode mode	100
0.5	SPE 2—3-electrode mode	70

alternative to the $[Ru(NH_3)_6]^{3+/2+}$ couple. DC cyclic voltammogramms obtained in 0.5 mM FcMeOH solution in 0.2 M KCl demonstrated reversible charge transfer behaviour with ΔE_p of 58 mV on GC electrode, 57 mV on SPE 1 and 62 mV on SPE 2 in three-electrode mode and also represents close to an ideal reversible model system.

The nominal electroactive electrode area was calculated from the forward (oxidative) sweep of cyclic voltammograms of 0.5 mM FcMeOH using the Randles–Sevcik equation. This also assumes diffusion to a planar electrode, which is a significant simplification. Cyclic voltammetric data derived from eight screen-printed type 1 electrodes in a three-electrode configuration gave an average electroactive electrode area of 2.69±0.10 mm^2 that was significantly smaller than the geometric area (3.16±0.10 mm^2 for the same eight electrodes). This difference may be a result of several factors such as the fact that the entire electrode surface was not accessible to the solution due to the particular design, which resulted in an uneven surface and possible well formation close to the outer part of the electrode (Fig. 1b) or blockage by binder, which meant that the planar diffusion model may not be valid. SPE 2, made by a different design and with the different inks, displayed an average electroactive electrode area of 0.608±0.020 mm^2 that was significantly larger than the geometric area (0.433±0.020 mm^2 for the same eight electrodes). Unlike the case with SPE 1, in SPE 2, the surface is more even with the carbon ink electrodes only slightly protruding above the dielectric layer. The fact that the electroactive area was larger than the geometric one was attributed to the roughness of the electrode surface. Despite their differences, the reproducibility was excellent in both cases of SPEs and significantly greater than that obtained in eight experiments with GC A electrodes polished between each experiment (7.2± 0.3 mm^2).

As described above, use of either $FcMeOH^{0/+}$ or $[Ru(NH_3)_6]^{3+/2+}$ processes and cyclic voltammetric studies of SPEs can be applied to ascertain some aspects of fabrication quality and reproducibility of single-use SPEs. Clearly, in terms of process control, Faradaic peak current, ΔE_p and R_u for a given set of parameters including FcMeOH or $[Ru(NH_3)_6]^{3+/2+}$ concentration needs to be reproducible with these mass-produced electrodes. High electrode resistance, variable capacitance and variable electrode area are characteristics of poor electrode manufacture. As will now be demonstrated, from a single experiment, FT AC voltammetry can rapidly provide details on the DC and AC Faradaic response, background capacitance (C) and resistance (R_s~R_u), which are parameters that can be related to quality control of mass-produced SPE performance as sensors [6, 18].

Determination of Faradaic current, electrode area, resistance and capacitance for quality control purposes using Fourier transformed AC voltammetry with a GC electrode

FT AC voltammetry was performed using five simultaneously applied sine waves, which is effectively equivalent to a series of experiments at different scan rates using DC cyclic voltammetry. The five sine waves had frequencies of 37.25, 92.54, 230.07, 373.05 and 590.09 Hz, each with the same amplitude of 5 mV. The power spectrum derived from a typical experiment is shown in Fig. 2d and confirms the presence of higher harmonic and frequency sum and frequency difference terms, which are filtered out when undertaking the inverse FT operation. The DC potential was scanned at a known rate, and the potential range was centred on the region where either $FcMeOH^{0/+}$ or $[Ru(NH_3)_6]^{3+/2+}$ process occurred. Fourier transformation was used to obtain the power spectrum, followed by inverse Fourier transformation of specific frequency bands, which separated the data into resolved DC and the required AC components at the five applied sine wave frequencies.

Initially, the proposed quality control procedure was examined with respect to GC A electrode. Traditionally, R_s and C values are determined in the absence of Faradaic current. An example of FT data obtained in the absence of Faradaic redox couple at GC A electrode and with a scan rate of 104.31 mV s^{-1} is presented in Fig. 7. The DC component derived from the FT AC voltammetry under conditions of Fig. 7a exhibits a small background current at the initial potential of −0.2 V, which then increases to −0.4 μA at the switching potential of 0.5 V. The ringing present at the initial, switching and final potentials is an artefact of the Fourier transformation process [19]. Resistance and capacitance data were calculated over the potential range of −0.2 to 0.5 V, which correspond to a time range of 0.1–6.7 s. Data obtained in the initial 0.1 s were neglected so as to exclude spikes associated with the initial ringing. Magnitude and angle vs time plots were calculated (Fig. 7b and c) using Eqs. 11 and 12 (see Appendix). Both the amplitude and phase vary with the applied DC potential. Mapping the amplitude and phase to the simple RC model suggests that both the R_s and C also vary slightly with applied DC potential (Fig. 7d). For the GC A electrode, values (± specific range) for the presented set of data were R_s=202±19 Ω and C=470±15 nF (Fig. 7d). The small dependence of R_s on potential confirms that the model of a simple RC circuit is not strictly correct. The variation of approximately 10% in the capacitance value with applied potential may be due to the variation in the double layer or surface functionality. The average values for R_s and C obtained at GC A (based on eight repetitions) were 262±54 Ω and 551±100 nF, respectively (Table 2).

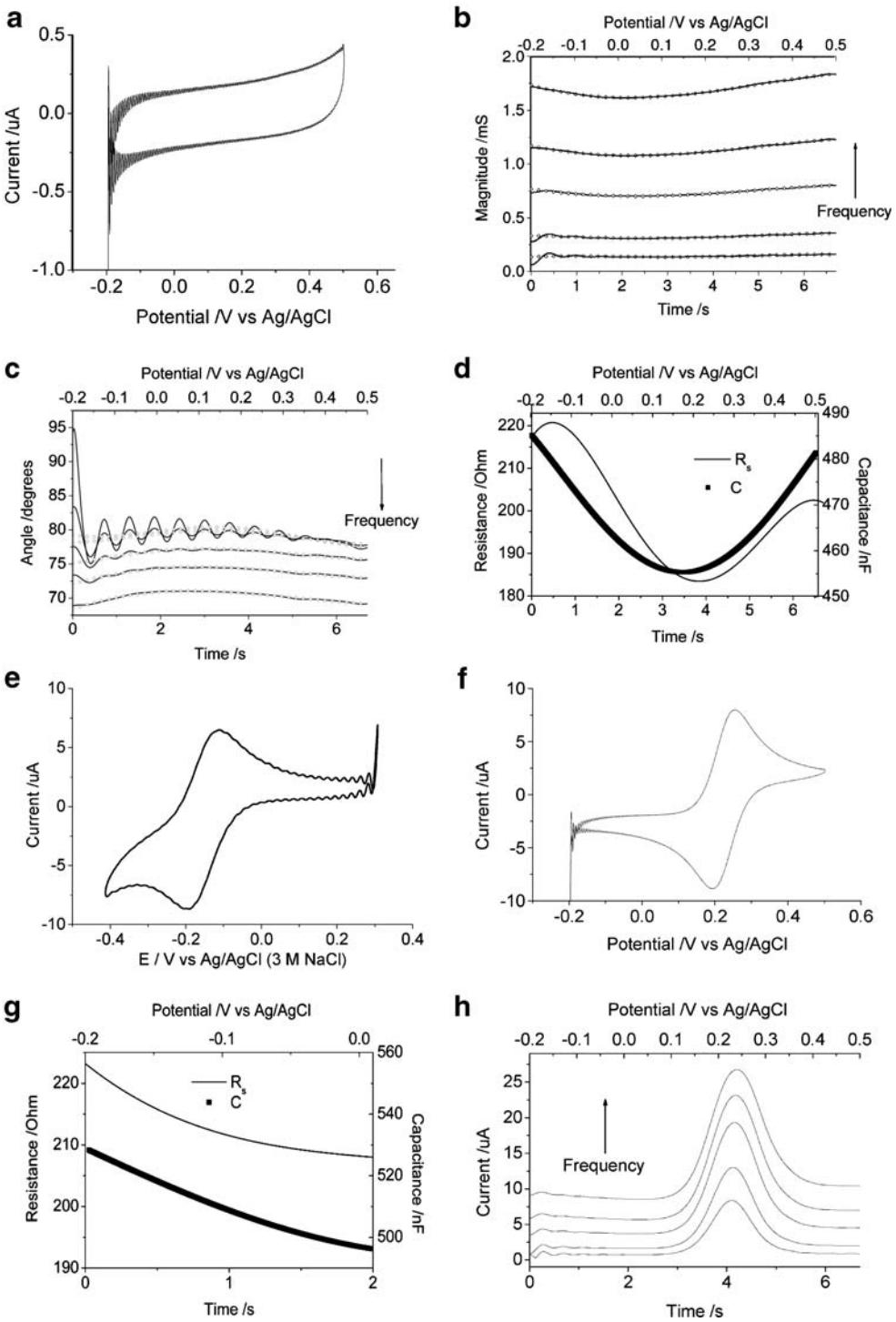

Fig. 7 FT AC voltammetry (37.25, 92.54, 230.07, 373.05 and 590.09 Hz, 5 mV amplitude) at a GC A working electrode in a three-electrode configuration at a scan rate of 104.31 mV s^{-1} for **a**–**d** 0.2 M KCl **e** with 0.5 mM $[Ru(NH_3)_6]Cl_3$ and **f**–**h** with 0.5 mM ferrocenemethanol added. **a**, **e**, **f** DC component; **b** magnitude; **c** angle; **d**, **g** resistance and capacitance values and **h** AC fundamental harmonic components obtained at GC B

Ideally, Faradaic current (electroactive electrode area), R_s and C in the quality control set-up should be assessed from a single experiment. To assess if R_s and C values could still be determined in the presence of Faradaic current, 0.5 or 5 mM $[Ru(NH_3)_6]^{3+/2+}$ or 0.5 mM FcMeOH was added to the 0.2 M KCl electrolyte solution. In this case, the background resistance and capacitance were calculated over times of 0.1–2 s, which corresponds to initial scan data obtained over the potential range of 0.3 to 0.1 V for $[Ru(NH_3)_6]^{3+/2+}$ or −0.2 to 0.01 V in the case of FcMeOH and again avoids the potential (time) regions associated with the initial charging current and significant redox voltammetry (and oxygen reduction in the case of $[Ru(NH_3)_6]^{3+/2+}$) (Fig. 7e,f). The example of estimated resistance and capacitance in the case of 0.5 mM FcMeOH is presented in Fig. 7g. The average values of resistance and capacitance

Table 2 FT AC voltammetric characterisation of GC A and SPEs

Electrode configuration	Experimental system, R_s and C					
	0.2 M KCl		0.2 M KCl 0.5 mM $[Ru(NH_3)_6]Cl_3$		0.2 M KCl 5 mM $Ru(NH_3)_6]Cl_3$	
	R_s/Ω (%SD)	C/nF (%SD)	R_s/Ω (%SD)	C/nF (%SD)	R_s/Ω (%SD)	C/nF (%SD)
GC A 3-electrode mode	262 (20)	551 (18)	265 (19)	541 (13)	440 (23)	554 (13)
SPE 1 2-electrode mode	858 (6)	73 (7)	958 (3)	68 (2)	830 (6)	71 (3)
SPE 1 3-electrode mode	429 (11)	89 (6)	381 (13)	93 (5)	445 (11)	68 (10)
SPE 2 2-electrode mode	6,930 (5)	13 (4)	7,575 (8)	13 (4)	6,700 (7)	13 (4)
SPE 2 3-electrode mode	3,820 (13)	13 (4)	4,125 (7)	13 (4)	3,955 (13)	13 (4)

obtained at GC A based on eight repeated experiments in 0.5 mM $[Ru(NH_3)_6]^{3+/2+}$ calculated in this manner were 265±50 Ω and 541±70 nF (75.1±9.7 mF mm^{-2}), respectively (Table 2).

Next, the GC electrode used extensively in our laboratory for over 3 years (GC B) was characterised according to the procedure described above. Cyclic voltammetry of this electrode repeated eight times with polishing between each experiment gave an average electroactive electrode area of 8.25±0.36 mm^2. Visual analysis of the electrode tip under a microscope revealed that the GC disc of the electrode was protruding above the Teflon holder, presumably due to extensive polishing over several years of usage. That resulted in the actual geometric and electroactive area being larger than the geometric area reported by the manufacturer (7.065 mm^2). The area of the GC B electrodes determined using the DC component of the FT data obtained in 0.5 mM ferrocene methanol solution and applying the Randles–Sevcik equation in a three-electrode mode was 8.09±0.24 mm^2 (compared to 8.25±0.36 mm^2 obtained from DC cyclic voltammetric experiments) (Table 3). Resistance and capacitance of GC B were determined in 0.5 mM FeMeOH solution using the same procedure as described above. The average values of resistance and capacitance for GC B based on eight experiments were 211±42 Ω and 754±294 nF (approx. 91.4 mF mm^{-2}), respectively (Table 3). The resistance value obtained is similar to that obtained with GC A, but the estimated capacitance value has a much higher level of variability in case of GC B. The larger variability in estimated capacitance is associated with highly variable functionalisation of the GC B electrode during the polishing step of the now curved surface.

Figure 7h illustrates FT AC voltammograms for each of the fundamental harmonics associated with the five applied frequencies. The relative contributions of background and Faradaic current at each frequency are readily seen. The Faradaic peak current of the fundamental harmonic obtained on GC B electrode, despite the irregular geometry of the electrode, displays a linear correlation with the square root of the applied frequency ($\omega^{1/2}$), indicating that the Faradaic process remains reversible. That is, the electrode is acting as a macrodisc at these applied frequencies and obeys the Nernst equation [20]. Comparison of single frequency data with these five frequency experiments shows slightly smaller AC peak currents for the multiple-frequency case, which is attributed to the third-order frequency sum and difference terms slightly reducing the power of the applied frequencies. Furthermore, the non-linearity of the background current with frequency suggests that the background is not purely capacitive, and the slightly larger peak widths at half height (approximately 100 mV) vs the theoretically expected 90 mV suggest that the $FcMeOH^{0/+}$ voltammetry contains a small level of surface catalysis, which is more significant at high frequencies [21] (O'Mullane A, Bond AM unpublished results). Consequently, electrode area analysis of the five AC harmonics is best confined to the lowest frequency data.

Table 3 FT AC voltammetric characterisation of GC B and SPEs in 0.2 M KCl and 0.5 mM ferrocenemethanol in a three electrode configuration

	GC B	SPE 1	SPE 2
$I_p$dc /μA (%SD)	10.0 (2.48)	3.27 (3.74)	0.737 (2.64)
$I_p$ac-37.25 Hz /μA (%SD)	7.94 (7.92)	3.20 (3.48)	0.570 (3.90)
Electroactive area (A_{el})/mm^2 (%SD)	8.25 (4.36)	2.68 (2.97)	0.608 (2.64)
R_s/Ω (%SD)	211 (20.2)	455 (7.30)	4,300 (9.29)
C/nF (%SD)	754 (39.2)	95.6 (3.43)	15.7 (2.51)
C/A_{el}/mF/m^2	91.4	35.7	25.8

To avoid problems with the oxygen reduction process, only FT data obtained in 0.5 mM FcMeOH were used for simulations. Good fits with experimental data generated on GC B were obtained using simulation parameters as follows: diffusion coefficient=7.6×10^{-6} cm^2 s^{-1} [22], concentration=0.5 mM, reversible process (electron transfer rate=10^5 cm s^{-1}), A=8.04 mm^2, C=70 mF m^{-2} and R_u= 80 Ω. (Fig. 8) The resistance value used in this simulation is smaller than R_s estimated earlier, again indicating the difference between R_u and R_s and illustrating that the use of the two-parameter RC model does not perfectly describe the non-Faradaic region. The significance of the resistance value estimated by the RC model was evaluated by adding external resistors in series to GC A electrode. Addition of a 510 Ω resistor resulted in an increase in estimated resistance (R_s) of 578 Ω (from 212 to 790 Ω), while addition of a 1.00 kΩ resistor resulted in an increase in R_s= 1.48 kΩ (to 1.67 kΩ). This result implied that estimated resistance (R_s) using the two-parameter model is higher than the value of the uncompensated resistance (R_u). However, as noted above, for quality-control purposes, it is the reproducibility in electrode manufacture that is the main focus. It is of course possible to use more sophisticated equivalent circuit models to analyse data, but for the purposes of quality control of electrode fabrication, where reproducibility is of particular importance, the simple RC circuit approach described above is considered entirely adequate.

The above results suggest that a basis of a protocol is now available to establish a procedure for quality control of mass-produced SPEs. Based on the analysis of FT AC voltammetric data, R_s and C can be obtained in a single experiment. Faradaic data can also be obtained from the same experiment and used to estimate electroactive electrode areas and their reproducibility. Values of each of these parameters in single-use SPE experiments should be highly reproducible, with significant deviations suggesting poor quality control during their manufacture.

Quality control assessment of SPEs

The FT AC voltammetry of the screen-printed disc electrodes was tested using the protocol applied above to the GC electrode. As noted above, because there is a cost incentive in using sensor electrodes in a two-electrode configuration, FT AC voltammetry was applied in both the two- and three-electrode modes.

The C, R_s and Faradaic current for screen-printed disc electrodes can be derived in exactly the same way as for the GC electrode via analysis of FT AC voltammetric data. In this case, measured resistance and capacitance values were again similar in both the presence and absence of Faradaic current derived from the $[Ru(NH_3)_6]^{3+/2+}$ process (Table 2). For SPE 1, analysis of FT AC data in the two-electrode mode configuration gave R_s and C values of 880 Ω and 70 nF, respectively. In contrast, a three-electrode configuration gave approximate R_s and C values of 420 Ω and 83 nF. As the contribution of solution resistance is small, this result implies that the resistances of the reference and working electrodes are similar because the value of R_s approximately doubles when a two-electrode mode is used. This is expected from the electrode design (Fig. 1) with resistance of the electrode legs and contact resistance to be similar. The absence of the silver track underneath the carbon ink resulted in much higher R_s values in both the two- and three-electrode configurations (Table 2) [17]. It is noteworthy that the C values for both types of SPEs (with and without silver) obtained in two- and three-electrode modes were essentially the same, indicating no apparent cross talking between reference and working electrodes in the two-electrode configuration. Very similar values were obtained when the experiments were conducted in the more positive potential region using the $FeMeOH^{0/+}$ redox couple (Table 3). Notably, the reproducibility of values obtained from single-use SPEs was higher than on the GC electrodes due to the removal of the polishing step. Interestingly,

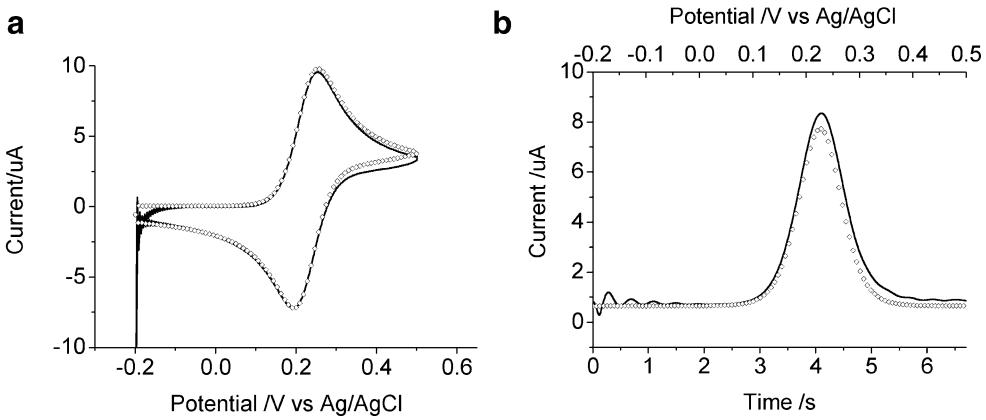

Fig. 8 **a** DC component of FT AC voltammetry (37.25, 92.54, 230.07, 373.05 and 590.09 Hz, 5 mV amplitude) and **b** AC fundamental harmonic component at 37.25 Hz at GC B using scan rate of 104.31 mV s^{-1} for oxidation of 0.5 mM ferrocenemethanol (0.2 M KCl) in a three-electrode configuration. *Line*, experimental data; *diamonds*, simulation. See text for details

despite the higher resistance of SPE 2, their reproducibility was better than SPE 1, as the print registration was superior. The electroactive area determined in 0.5 mM FeMeOH for eight SPE 1 was 2.68±0.08 vs 2.69±0.10 mm^2, and that for eight SPE 2 was 0.608±0.01 vs 0.608±0.02 mm^2 from the DC component of the FT voltammetry and DC cyclic voltammetry experiments, respectively (Table 3).

Simulation of the $FeMeOH^{0/+}$ process for FT AC voltammetry at SPE 1 provided a good fit to experimental data using A=2.78 mm^2, C=35 mF m^{-2} and R_u=50 Ω (Fig. 9). Simulation of electrode 2 was performed with A=0.61 mm^2, C=28 mF m^{-2} and R_u=1,900 Ω (Fig. 10). Again, the R_u values were smaller than R_s estimated via the two-parameter RC model circuit. However, estimated capacitance matched well with the value used for simulation (Table 3). Upon adding additional resistance in series and using the FT RC model of analysis, it was observed that, with SPE 1 in two-electrode mode, addition of a 510-Ω resistor resulted in an estimated resistance (R_s) increase of 706±100 Ω (1.54±0.1 kΩ from initial 834±50 Ω), while addition of a 1-kΩ resistor resulted in an estimated resistance (R_s) increase of 1.44±0.2 kΩ (up to 2.28±0.2 kΩ). Clearly, the resistance added was overestimated using the two-parameter RC model. However, as emphasised in this paper, the values (R_s) generated using the two-parameter RC model are adequate for quality control purposes. In practice, studies with more than 100 SPE 1 and 2, using the five-frequency waveform with RC analysis, generated electroactive area, R_s, C and DC and AC peak current values, which were invariably in the range of the data presented in Table 3. Thus, 3% reproducibility of DC and AC peak current is readily achievable with SPEs. Very rarely (less than 1 in 250), poor-quality electrodes were manufactured. Very high resistance, low DC and AC peak currents and capacitance are indicative of low electroactive area and/or poor contact and are easily identified using the protocol suggested.

Conclusions

Mass-produced, screen-printed, carbon ink-based disc electrodes that are widely used for glucose and other kinds of sensing applications need to be assessed for their reproducibility of manufacture. Characterisation by surface techniques indicated high heterogeneity of the electrode surface. The data presented demonstrate the necessity of experimental determination of the electroactive area of the electrode that cannot be assumed to be equal to the geometrical one due to various manufacturing and design factors. Use of a FT AC voltammetric protocol developed in this work enables resistance, as well as capacitance and DC and AC Faradaic currents, derived from a reversible process such as $FcMeOH \rightleftarrows FcMeOH^+ + e^-$, to be assessed from a single experiment. Because of the potential impact of oxygen reduction on the data obtained using reduction of $[Ru(NH_3)_6]^{3+}$, ferrocene methanol is recommended for routine quality control assessment.

The simple protocol involves application of a waveform derived from a DC ramp and five superimposed sine waves of different frequency but the same amplitude. The resistance and capacitance terms are derived from analysis of data collected in a potential region where no Faradaic current is present, and use of a model based on a simple RC circuit. The DC and AC Faradaic peak currents that assay the reproducibility of the electroactive area are derived from use of a FT-inverse FT sequence. The protocol developed is recommended for routine SPE batch calibration.

Data obtained in this study imply that screen-printed carbon macrodisc electrodes are relatively easy to manufacture in a configuration where, despite their heterogeneous surface, R_s, C and the Faradaic responses meet reproducibility levels required for applications in aqueous electrolyte media. Comparison with data obtained at commercial multi-used GC electrodes indicates that the SPEs may be more reproducible with respect to capaci-

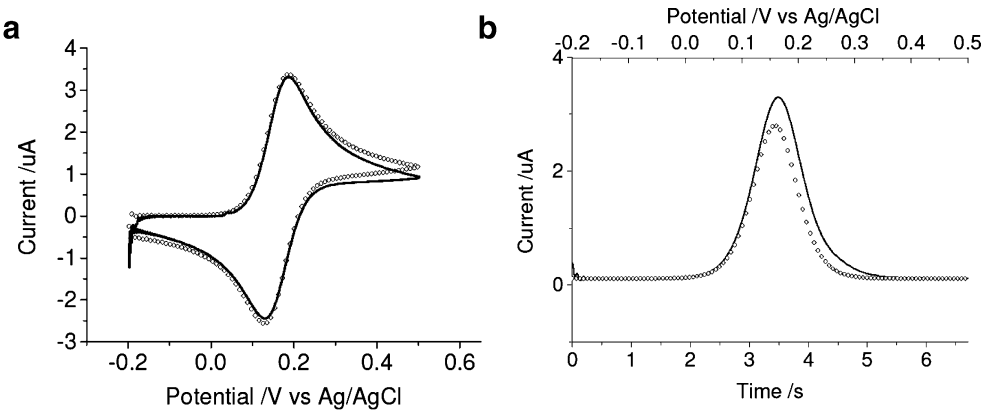

Fig. 9 **a** DC component of FT AC voltammetry (37.25, 92.54, 230.07, 373.05 and 590.09 Hz, 5 mV amplitude) and **b** AC fundamental harmonic component at 37.25 Hz at SPE 1 at a scan rate of 104.31 mV s^{-1} for oxidation of 0.5 mM ferrocenemethanol (0.2 M KCl) in a three-electrode configuration. *Line*, experimental data; *diamonds*, simulation. See text for details

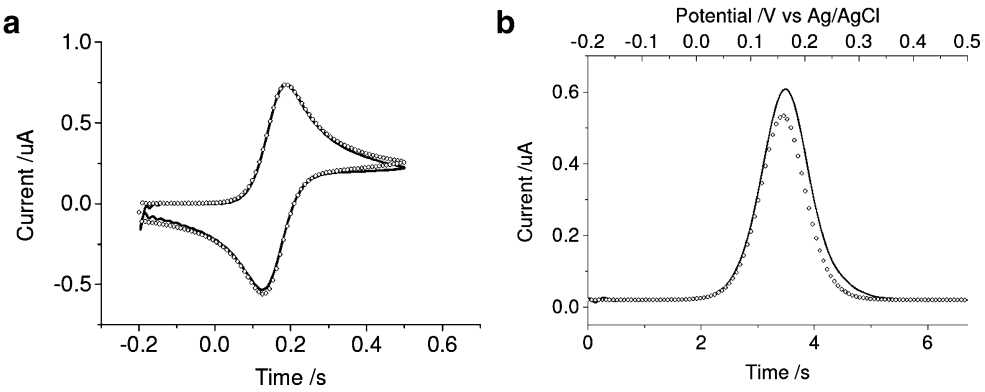

Fig. 10 **a** DC component of FT AC voltammetry (37.25, 92.54, 230.07, 373.05 and 590.09 Hz, 5 mV amplitude) and **b** AC fundamental harmonic component at 37.25 Hz at SPE 2 at a scan rate of 104.31 mV s^{-1} for oxidation of 0.5 mM ferrocenemethanol (0.2 M KCl) in a three-electrode configuration. *Line*, experimental data; *diamonds*, simulation. See text for details

tance, as the polishing step needed in re-use of GC electrodes can produce a variable level of functionalisation of their surface. The reproducibility of the Faradaic current is also higher at SPEs, and with careful design, the error can be brought down to ≤3%.

Appendix

Derivation of the equations to calculate resistance and capacitance values

To use the FT AC voltammetric approach for quality control purposes, it was assumed that R_u and C values of SPEs could be derived from the data obtained in a potential region where there is no Faradaic current and use of the simplest possible equivalent circuit (Fig. 3), where resistor (R_s) and capacitor (C) are connected in series. It is noteworthy that R_s is not necessarily equal to R_u and should be used only as an approximation of the R_u value. Nevertheless, easily acquired R_s values are appropriate for quality control purposes. Under assumptions detailed in references [9–12], for each of the frequency components applied during an FT AC voltammetric experiment, admittance (Y) [magnitude ($|Y|$) and angle ($\angle Y$)] values may be calculated from relationships developed in Eqs. 6a–15f.

For the fundamental harmonic of a given perturbation frequency (ω), the current (I) and voltage (V) with amplitude (A and B) and phase (ϕ and γ) exhibit the general time (t)-dependant relationships:

$$I(t) = A(t)\sin(\omega t + \phi(t)) \tag{6a}$$

$$V(t) = B(t)\sin(\omega t + \gamma(t)) \tag{6b}$$

The current and voltage are then multiplied by $\sin(\omega t)$ and $\cos(\omega t)$, resulting in the following four components:

$$\begin{aligned} I(t)\times\sin(\omega t) &= A(t)\sin(\omega t+\phi(t))\cdot\sin(\omega t)\\ &= \frac{A(t)}{2}\cos(\phi(t)) - \frac{A(t)}{2}\cos(2\omega t+\phi(t)) \end{aligned} \tag{7a}$$

$$\begin{aligned} I(t)\times\cos(\omega t) &= A(t)\sin(\omega t+\phi(t))\cdot\cos(\omega t)\\ &= \frac{A(t)}{2}\sin(\phi(t)) + \frac{A(t)}{2}\sin(2\omega t+\phi(t)) \end{aligned} \tag{7b}$$

$$\begin{aligned} V(t)\times\sin(\omega t) &= B(t)\sin(\omega t+\gamma(t))\cdot\sin(\omega t)\\ &= \frac{B(t)}{2}\cos(\gamma(t)) - \frac{B(t)}{2}\cos(2\omega t+\gamma(t)) \end{aligned} \tag{7c}$$

$$\begin{aligned} V(t)\times\cos(\omega t) &= B(t)\sin(\omega t+\gamma(t))\cdot\cos(\omega t)\\ &= \frac{B(t)}{2}\sin(\gamma(t)) + \frac{B(t)}{2}\sin(2\omega t+\gamma(t)) \end{aligned} \tag{7d}$$

The high-frequency components ($2\omega t$ terms) are removed using a FT low-pass filter, resulting in real and imaginary current and voltage terms:

$$I_{\text{Real}} = \frac{A(t)}{2}\cos(\phi(t)) \tag{8a}$$

$$I_{\text{Imaginary}} = \frac{A(t)}{2}\sin(\phi(t)) \tag{8b}$$

$$V_{\text{Real}} = \frac{B(t)}{2}\cos(\gamma(t)) \tag{8c}$$

$$V_{\text{Imaginary}} = \frac{B(t)}{2}\sin(\gamma(t)) \tag{8d}$$

These equations can be rewritten in the form:

$$I = I_{\text{Real}} + jI_{\text{Imaginary}} = \frac{A(t)}{2}(\cos(\phi(t)) + j\sin(\phi(t))) = \frac{A(t)}{2}e^{j\phi(t)} \tag{9a}$$

$$V = V_{\text{Real}} + jV_{\text{Imaginary}} = \frac{B(t)}{2}(\cos(\gamma(t)) + j\sin(\gamma(t))) = \frac{B(t)}{2}e^{j\gamma(t)} \tag{9b}$$

Admittance (Y) is calculated by combining Eqs. 9a and 9b:

$$Y = \frac{I}{V} = \frac{A(t)}{B(t)} \cdot e^{j(\phi(t)-\gamma(t))} \tag{10}$$

Magnitude ($|Y|$) and angle components ($\angle Y$) of admittance can then be directly determined as:

$$|Y(t)| = \frac{A(t)}{B(t)} \tag{11}$$

$$\angle Y(t) = \phi(t) - \gamma(t) \tag{12}$$

At a specific time, these terms are then used to obtain R_s and C values directly from Eqs. 13 and 14:

$$R_s = \frac{1}{\omega C \tan(\phi)} = \frac{1}{|Y|\sqrt{\tan^2(\phi)+1}} \tag{13}$$

$$C = \frac{1}{\omega}|Y|\sqrt{1+\frac{1}{\tan^2(\phi)}} \tag{14}$$

In this equation, C is the symbol that is used to represent total capacitance, which is assumed to be derived primarily from the double layer capacitance (C_{dl}), but may include contributions from other instrumental and stray terms, R_s is the resistance which is assumed to be in series to the capacitor.

Equations 13 and 14 were derived from analysis of the impedance (Z) of the equivalent circuit shown in Fig. 3, which gives the relationship summarised in Eqs. 15a–f:

$$Z = R_s + \frac{1}{j\omega C} \tag{15a}$$

$$Y = \frac{1}{Z} = \frac{1}{R_u + \frac{1}{j\omega C}} = \frac{j\omega C}{1 + j\omega R_s C} = \frac{j\omega C(1 - j\omega R_s C)}{1 + \omega^2 R_s^2 C^2} = \underbrace{\frac{\omega^2 R_s C^2}{1+\omega^2 R_s^2 C^2}}_{\text{Real}} + \underbrace{\frac{\omega C}{1+\omega^2 R_s^2 C^2}}_{\text{Imaginary}} j \tag{15b}$$

$$|Y| = \sqrt{\text{Real}^2 + \text{Imaginary}^2} = \sqrt{\frac{\omega^4 R_s^2 C^4}{\left(1+\omega^2 R_s^2 C^2\right)^2} + \frac{\omega^2 C^2}{\left(1+\omega^2 R_s^2 C^2\right)^2}} = \sqrt{\frac{\omega^2 C^2\left(1+\omega^2 R_s^2 C^2\right)}{\left(1+\omega^2 R_s^2 C^2\right)^2}} = \frac{\omega C}{\sqrt{1+\omega^2 R_s^2 C^2}} \tag{15c}$$

$$\phi = \tan^{-1}\left(\frac{\text{Imaginary}}{\text{Real}}\right) = \tan^{-1}\left(\frac{\omega C}{\omega^2 R_s C^2}\right) = \tan^{-1}\left(\frac{1}{\omega R_s C}\right) \tag{15d}$$

$$\frac{1}{\tan(\phi)} = \omega R_s C \tag{15e}$$

$$|Y| = \frac{\omega C}{\sqrt{1+\frac{1}{\tan^2(\phi)}}} \tag{15f}$$

The derivations are equivalent to those widely available in standard textbooks on electrochemistry [9–11]. It is, of course, recognised that carbon electrodes are actually complex, chemically modified electrodes (see text) and that the simple RC network used for the equivalent circuit analysis represents only a modest approximation of the actual situation. A theoretical description of more complex equivalent circuits is available [12]. However, in quality control, it is the reproducibility of the data rather than absolute values of resistance and capacitance that is critical, and so, the simple RC approach was adopted.

References

1. Galan-Vidal CA, Munoz J, Dominguez C, Alegret S (1995) TrAC Trends Anal Chem 14:225–231
2. Wang J (2002) TrAC Trends Anal Chem 21:226–232
3. Hart JP, Wring SA (1994) Electroanalysis 6:617–624
4. Hart JP, Crew A, Crouch E, Honeychurch KC, Pemberton RM (2004) Anal Lett 37:789–830
5. Green MJ, Hilditch PI (1991) Anal Proc (London) 28:374–376
6. Bond AM, Duffy N, Guo S-X, Zhang J, Elton D (2005) Anal Chem 77:186A–195A
7. Zhang J, Guo S-X, Bond AM, Marken F (2004) Anal Chem 76:3619–3629
8. Retter U, Lohse H (2002) In: Scholz F (ed) Electroanalytical methods: guide to experiments and applications. Springer, Berlin Heidelberg New York, pp 149–166
9. Bagotsky VS (2006) Fundamentals of electrochemistry. Wiley, Hoboken
10. Gileadi E (1993) Electrode kinetics for chemists, chemical engineering, and materials scientists. VCH, New York
11. Bard AJ, Faulkner LR (2001) Electrochemical methods. Wiley, New York
12. Pettit CM, Goonetilleke PC, Roy D (2006) J Electroanal Chem 589:219–231
13. Wang J, Tian B, Nascimento VB, Angnes L (1998) Electrochim Acta 43:3459–3465
14. Noh MFM, Kadara RO, Tothill IE (2005) Anal Bioanal Chem 382:1175–1186
15. Seddon BJ, Osborne MD, Lagger G, Dryfe RAW, Loyall U, Schaefer H, Girault HH (1997) Electrochim Acta 42:1883–1894
16. Osborne MD, Seddon BJ, Dryfe RAW, Lagger G, Loyal U, Schifer H, Girault HH (1996) J Electroanal Chem 417:5–15
17. Gilleo K (1996) Polymer thick film. Springer, Berlin Heidelberg New York
18. Sher AA, Bond AM, Gavaghan DJ, Gillow K, Duffy NW, Guo S-X, Zhang J (2005) Electroanalysis 17:1450–1462
19. Gavaghan DJ, Bond AM (2000) J. Electroanal Chem 480:133–149
20. Gavaghan DJ, Elton D, Bond AM (2001) Collect Czech Chem Commun 66:255–275
21. Zhang J, Bond AM (2007) J Electroanal Chem 600:23–34
22. Anicet N, Bourdillon C, Moiroux J, Saveant JM (1998) J Phys Chem B 102:9844–9849